Genomics Proteomics Bioinformatics 21 (2023) 1101–1116

Genomics Proteomics Bioinformatics

www.elsevier.com/locate/gpb
www.sciencedirect.com

ORIGINAL RESEARCH

Novel Time-dependent Multi-omics Integration in Sepsis-associated Liver Dysfunction

Ann-Yae Na [1,#], Hyojin Lee [2,#], Eun Ki Min [2], Sanjita Paudel [1,3], So Young Choi [1,3], HyunChae Sim [1,3], Kwang-Hyeon Liu [1,3], Ki-Tae Kim [2], Jong-Sup Bae [1,3], Sangkyu Lee [1,3,4,*]

[1] *Research Institute of Pharmaceutical Sciences, Kyungpook National University, Daegu 41566, Republic of Korea*
[2] *Department of Environmental Engineering, Seoul National University of Science and Technology, Seoul 01811, Republic of Korea*
[3] *BK21 FOUR Community-Based Intelligent Novel Drug Discovery Education Unit, College of Pharmacy, Kyungpook National University, Daegu 41566, Republic of Korea*
[4] *School of Pharmacy, Sungkyunkwan University, Suwon 16419, Republic of Korea*

Received 14 January 2022; revised 3 February 2023; accepted 11 April 2023
Available online 20 April 2023

Handled by Leng Han

KEYWORDS

Multi-omics;
Omics technology;
Sepsis-associated liver dysfunction;
Single omics;
Time-dependent integration

Abstract The recently developed technologies that allow the analysis of each **single omics** have provided an unbiased insight into ongoing disease processes. However, it remains challenging to specify the study design for the subsequent integration strategies that can associate sepsis pathophysiology and clinical outcomes. Here, we conducted a time-dependent **multi-omics** integration (TDMI) in a **sepsis-associated liver dysfunction** (SALD) model. We successfully deduced the relation of the Toll-like receptor 4 (TLR4) pathway with SALD. Although TLR4 is a critical factor in sepsis progression, it is not specified in single-omics analyses but only in the TDMI analysis. This finding indicates that the TDMI-based approach is more advantageous than single-omics analyses in terms of exploring the underlying pathophysiological mechanism of SALD. Furthermore, TDMI-based approach can be an ideal paradigm for insightful biological interpretations of multi-omics datasets that will potentially reveal novel insights into basic biology, health, and diseases, thus allowing the identification of promising candidates for therapeutic strategies.

Introduction

Sepsis, especially in its severe cases, induces multiple organ dysfunction as a result of systemic infections [1]. Globally, 20 million people are treated in hospitals for sepsis, a condition that causes as many as 5 million deaths each year (https://www.who.int/news-room/fact-sheets/detail/sepsis). The multiple organ dysfunction syndromes have been identified as a

* Corresponding author.
E-mail: sangkyu@skku.edu (Lee S).
# Equal contribution.

Peer review under responsibility of Beijing Institute of Genomics, Chinese Academy of Sciences / China National Center for Bioinformation and Genetics Society of China.

https://doi.org/10.1016/j.gpb.2023.04.002

major organ failure in patients with systemic inflammatory response syndrome. During sepsis, the liver removes bacteria and plays a vital role in the subsequent immune responses that produce inflammatory mediators. However, the liver also serves as a potential target of regulatory inflammatory responses. Sepsis-associated liver dysfunction (SALD) is considered a late feature of traditional critical illness that is characterized by jaundice and hyperbilirubinemia [2]. However, recent studies have revealed that liver dysfunction tends to occur early in the sepsis process [3]. Despite the numerous studies targeting sepsis, there is no specific treatment for patients with this condition, and the subsequent treatment relies solely on infection control, source removal, use of effective antibiotics, and organ function support [4]. Therefore, a novel research approach is needed for the identification of potential therapeutic clues that can help clinicians tackle this condition.

Omics technologies are defined as high-throughput biochemical assays, including genomics, transcriptomics, proteomics, and metabolomics, that have considerably advanced the possibility of personalized medicine as a tool to prevent and treat diseases [5]. Parallel to the advances in high-throughput biology, biomedical data analysis applications have facilitated the discovery of pathophysiological changes and targeting of novel therapeutic candidates [6,7]. Every single-omics analysis is a powerful analytical tool for studying gene expression in transcriptome profiling studies [8], complex protein metabolic interactions in proteome [9,10], and small molecules as compounds in metabolome [11,12]. However, the major limitation of classical omics studies is the isolation of only one level of biological complexity. For instance, metabolomics studies may provide information at the level of endogenous products, but many different entities may contribute to the biological state of metabolites, including genomic variants, post-transcriptional modifications, and protein–protein interactions [13]. Therefore, the integration of different multi-omics datasets can provide a notable insight into the complex molecular functional mechanisms involved by reinforcing complementary evidence from multiple levels [14]. This scenario makes it possible to critically appraise entire disease pathogenesis pathways rather than single-molecule associations [15]. Despite the introduction of a multi-omics technique platform, the integration of multi-omics datasets remains challenging due to the complexity of generating and analyzing statistical results [16].

Multi-omics data integration analyses may be used in various approaches [17–20]. For example, Canzler et al. showed that omics data selection strongly relies on the research purpose and model systems to enable the detection of response pathways under model conditions and optimally consider their response time in data of each omics [21]. Here, we integrated multiple levels of single-omics data (*e.g.*, transcriptome, phosphoproteome, proteome, and metabolome) in a different time-course of the early progression of SALD in a cecum ligation and puncture (CLP) model. To explore the molecular mechanisms underlying disease progression, the results of phosphoproteome at 4 h, transcriptome at 6 h, proteome at 18 h, and metabolome at 18 h were collected according to the central dogma. Time-dependent multi-omics integration (TDMI) was performed by combining the obtained single-omics data. To the best of our knowledge, this study is the first trial suggesting statistical pathways for integrative multi-omics data related to SALD. Given the increasing number of studies collecting multi-omics data with a limited methodological framework overview for integrative analyses [22–24], our approach will provide novel insights into sepsis development and SALD, along with novel tools that improve the diagnosis of this condition.

Results

SALD and inflammation response are induced by CLP surgery

Seven-week-old Institute of Cancer Research (ICR) male mice (n = 6) were used to induce SALD by a CLP surgery (**Figure 1**A). Sera and liver tissues were prepared at 0 h, 4 h, 6 h, 15 h, and 18 h after CLP surgery. Liver injury levels in sera and liver tissues were assessed to explore the pathogenesis of sepsis with liver dysfunction. Blood biochemical parameters [*i.e.*, serum aspartate transaminase (AST), alanine transaminase (ALT), alkaline phosphatase (ALP), and lactate dehydrogenase (LDH)] from ICR mice of two groups that were subjected to CLP 6 h and 18 h before the experiments were evaluated (Figure S1A). Serum AST and LDH were significantly higher at 18 h after surgery in the CLP group than in the control group (0 h). Inflammation levels were confirmed by sepsis progression according to the SALD time-course. Immunoblotting was used to clarify the production of cytokines after the CLP surgery (Figure 1B, Figure S1B). These results indicate an increase in the protein levels of high-mobility group box 1 (HMGB1), phospho-nuclear factor-κB p65 (pNF-κB p65), and interleukin 6 (IL-6) at 4 h followed by a gradual decrease after 6 h. The only exception was IL-6, which was strongly expressed up to 18 h after the CLP surgery. In addition, the expression levels of inflammatory cytokines such as tumor necrosis factor-α (TNF-α) and IL1-β were increased at 4 h and 6 h after CLP, respectively (Figure 1B).

Hematoxylin and eosin (H&E) stains of liver tissue samples were analyzed by a microscope (magnification, ×400) to examine the histopathological changes in the liver of mice with sepsis (Figure 1C). Quantification of granulocytes in the liver showed focal inflammatory cell infiltration at 6 h and 18 h after CLP (thick black arrows) and granulocytes in the sinusoids at 18 h after CLP (green arrows). Liver injury was defined as the amount of destructed hepatic lobules, infiltration of inflammatory cells, hemorrhage, and hepatocyte necrosis. The severity of injury was scored from 1 to 4 according to the percentage area of involvement per high power field (HPF). The liver injury increased significantly in the 18-h CLP group of mice compared with the 0-h control group (Figure S1C).

Phosphoproteomic analysis reveals association of pyruvate metabolism with SALD

First, we performed Western blotting using pan-anti-serine (Ser)/threonine (Thr)/tyrosine (Tyr) phospho-antibodies in the livers obtained after CLP surgery (Figure S2A), and we observed the changes in protein phosphorylation throughout the SALD progress. In the case of phosphoserine (pSer), the signal increased up to 18 h post-surgery. Neither phosphothreonine (pThr) nor phosphotyrosine (pTyr) remained constant, but as CLP progressed, an increase or decrease in proteins with

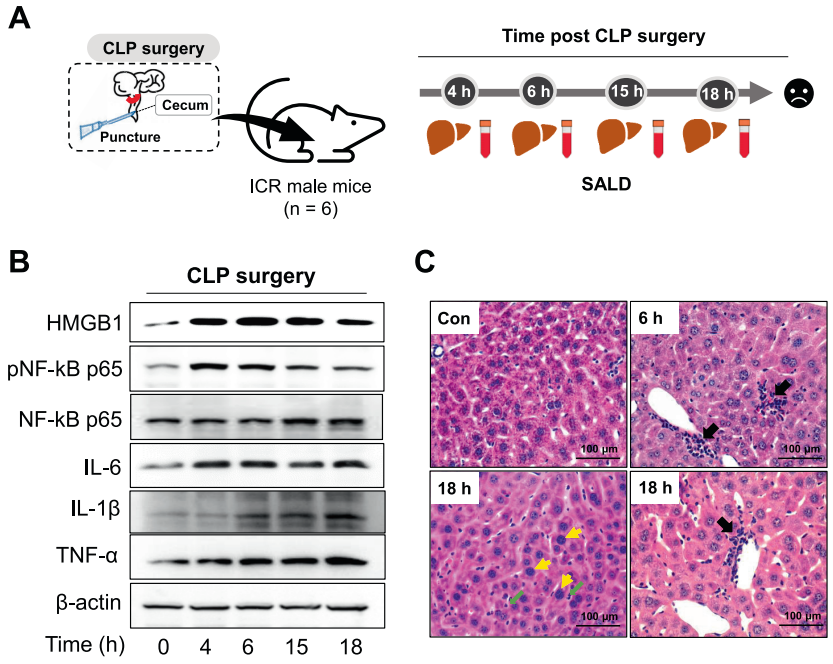

Figure 1 Overall scheme for the time-course omics analysis according to SALD

A. SALD was induced in ICR male mice (n = 6) by CLP surgery, and blood and livers were prepared at 0 h, 4 h, 6 h, 15 h, and 18 h after the CLP surgery. **B.** Western blotting of inflammatory factors indicating SALD. **C.** H&E staining of the liver from mice at 0 h, 6 h, and 18 h after the CLP surgery. Scale bar, 100 μm. The thick black arrows indicate the focal inflammatory cell infiltration (at 6 h and 18 h), green arrows indicate the granulocytes in the sinusoids (at 18 h), and yellow arrows indicate the hepatocytes with enlarged nuclei (karyomegaly, at 18 h). SALD, sepsis-associated liver dysfunction; CLP, cecum ligation and puncture; H&E, hematoxylin and eosin; HMGB1, high-mobility group box 1; pNF-κB p65, phospho-nuclear factor-κB p65; NF-κB p65, nuclear factor-κB p65; IL, interleukin; TNF, tumor necrosis factor; ICR, Institute of Cancer Research; Con, control.

different molecular weights was observed. When summarizing the results, phosphorylation commonly started to change at 4 h compared with 0 h for pSer, pThr, and pTyr. We performed quantitative phosphoproteomic analysis based on titanium dioxide (TiO_2) phosphopeptide enrichment technology coupled with tryptic digestion in ^{16}O or ^{18}O labeled water (**Figure 2**A) to understand the signaling process in the liver at the early stages of sepsis. All experimental samples were in biological replicates, and Pearson correlation coefficient showed $r = 0.886$ (Figure S2B). We identified 2462 phosphosites of which 1441 were quantified. Among the normalized phosphosites, compared with the respective global proteins, 79 (12.3%) and 163 (25.4%) phosphosites were up- and down-regulated in 640 phosphoproteins in the 4-h CLP mice, respectively, compared with the 0-h control group, based on fold change (FC) ≥ 1.5 or ≤ 0.666 (Table S1). We then carried out a one-way *t*-test with Perseus to detect the statistically significantly differentially expressed phosphorylated proteins (DEPPs; FC ≥ 1.5 or ≤ 0.666, $P < 0.05$), and the results showed that 19 up-regulated and 34 down-regulated phosphoproteins changed significantly in the 4-h CLP group (Figure 2B; Table S2).

Using Fisher's exact test, we performed annotation enrichment analyses of the up-/down-regulated phosphoproteins (FC ≥ 1.5 or ≤ 0.666) in the 4-h CLP group against the 0-h control group. The Kyoto Encyclopedia of Gene and Genomes (KEGG) pathway enrichment analysis showed that up-regulated phosphoproteins were enriched for RNA transportation and pyruvate metabolism pathways, while down-regulated phosphoproteins were enriched for antibiotics biosynthesis and carbon metabolism pathways (Figure 2C). Among the phosphoproteins involved in pyruvate metabolism, a 6.54-fold increase in phosphorylation at S232 of pyruvate dehydrogenase E1 (PDHE1, EC 1.2.4.1) was identified in the 4-h CLP group, suggesting that S232 phosphorylation of PDHE1 is *PDK1*-dependent and widespread across tissues (Table S2) [25]. The up-regulated phosphoproteins in the 4-h CLP group were associated with the poly(A) RNA binding in Gene Ontology molecular function (GOMF), nucleoplasm in Gene Ontology cellular component (GOCC), and translational initiation in Gene Ontology biological process (GOBP) (Figure S3). In contrast, the down-regulated phosphoproteins in the 4-h CLP group were associated with cadherin binding related to cell–cell adhesion in GOMF, cytoplasm in GOCC, and cell–cell adhesion in GOBP (Figure S3).

Transcriptomic analysis reveals association of altered *ApoE* with SALD

Next, we performed transcriptomic analysis on livers acquired at 6 h and 18 h after CLP surgery to analyze gene expression changes related to SALD progression after sepsis was induced. For quality check after RNA sequencing (RNA-seq), 15,323 genes were analyzed by removing zero value of fragments per kilobase of transcript per million mapped reads (FPKM) and quantile normalization to minimize the systematic bias between samples using the $\log_2$-transformed scale (Table S3).

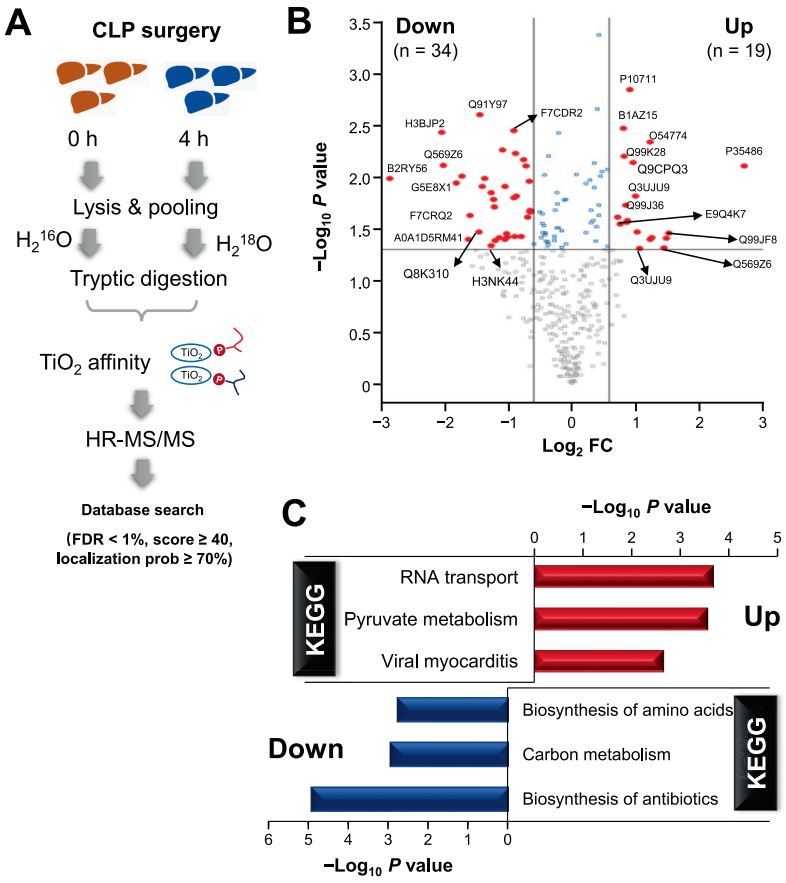

Figure 2 Comparative phosphoproteomic profiling in SALD

A. Experimental scheme of phosphophroteomic profiling. **B.** Volcano plot showing the significant DEPPs in the 4-h CLP group compared with the 0-h control group. Significantly changed phosphoproteins are marked with red color (up-regulated DEPPs, n = 19; down-regulated DEPPs, n = 34). FC $\geq$ 1.5 or $\leq$ 0.666; $P < 0.05$ (one-way *t*-test). **C.** Enriched KEGG pathways of up-/down-regulated phosphoproteins (FC $\geq$ 1.5 or $\leq$ 0.666) identified in the 4-h CLP group. Red colored and blue colored bar graphs were created by the up-regulated and down-regulated phosphoproteins. FC, fold change; KEGG, Kyoto Encyclopedia of Gene and Genomes; DEPP, differentially expressed phosphorylated protein; FDR, false discovery rate; HR-MS/MS, high-resolution tandem mass spectrometry.

The degree of similarity between samples (Pearson correlation coefficient) can be examined using the normalized value of each sample to determine whether the repeated sample is reproducible (range: $-1 \leq r \leq 1$). The closer the *r* values for all samples were to 1, the higher their respective similarity (Figure S4A). For each sample, a multidimensional scaling (MDS) plot of distribution using normalized values was performed among the groups, which was expressed in a two-dimensional space using the two components that best described the variability of the overall data (Figure S4B). We visualized the functional Gene Ontology (GO) terms of transcriptome in a heatmap of the one-way hierarchical clustering using z-scores for the normalized values (Figure S4C) to reveal quantitative transcriptome in dynamic responses according to the progression of sepsis. These results showed similar expression patterns between two sample groups.

The number of genes with altered expression levels (up-regulated, FC $\geq$ 2.0; down-regulated, FC $\leq$ 0.5) was determined (**Figure 3**A) to explore the transcriptomic functional profiling. In the 6-h CLP group, 778 up-regulated and 740 down-regulated genes were analyzed. In the 18-h CLP group, 795 up-regulated and 915 down-regulated genes were analyzed. Among these up-/down-regulated genes, the top 5 genes with respect to FC and volume in the 6-h CLP group were the apolipoprotein E (*ApoE*) gene (up-regulated) and the genes from the *Mup* family (*Mup1*, *Mup9*, *Mup12*, and *Mup17*; down-regulated) (Figure 3B). Previous studies have found a vital correlation between the increase in ApoE in the liver and the increase in sepsis-induced mortality with concomitant hepatic natural killer T (NKT) cell proliferation and activation [26,27]. In our study, we observed that the expression of *ApoE* increased significantly ($P < 0.05$) in the liver during the early sepsis stages, and thus it could be an important key regulator in inhibiting early sepsis progression. The functional classification and gene annotation were carried out based on GO information for differentially expressed genes (DEGs; FC $\geq$ 2.0 or $\leq$ 0.5, $P < 0.05$) (Figure 3C). The "binding" and "catalytic activity" annotations were enriched in GOMF, and the "intracellular" and "cellular anatomical entity" were highly enriched in GOCC. The "positive regulation of cellular process" and "response to stress" were enriched in GOBP.

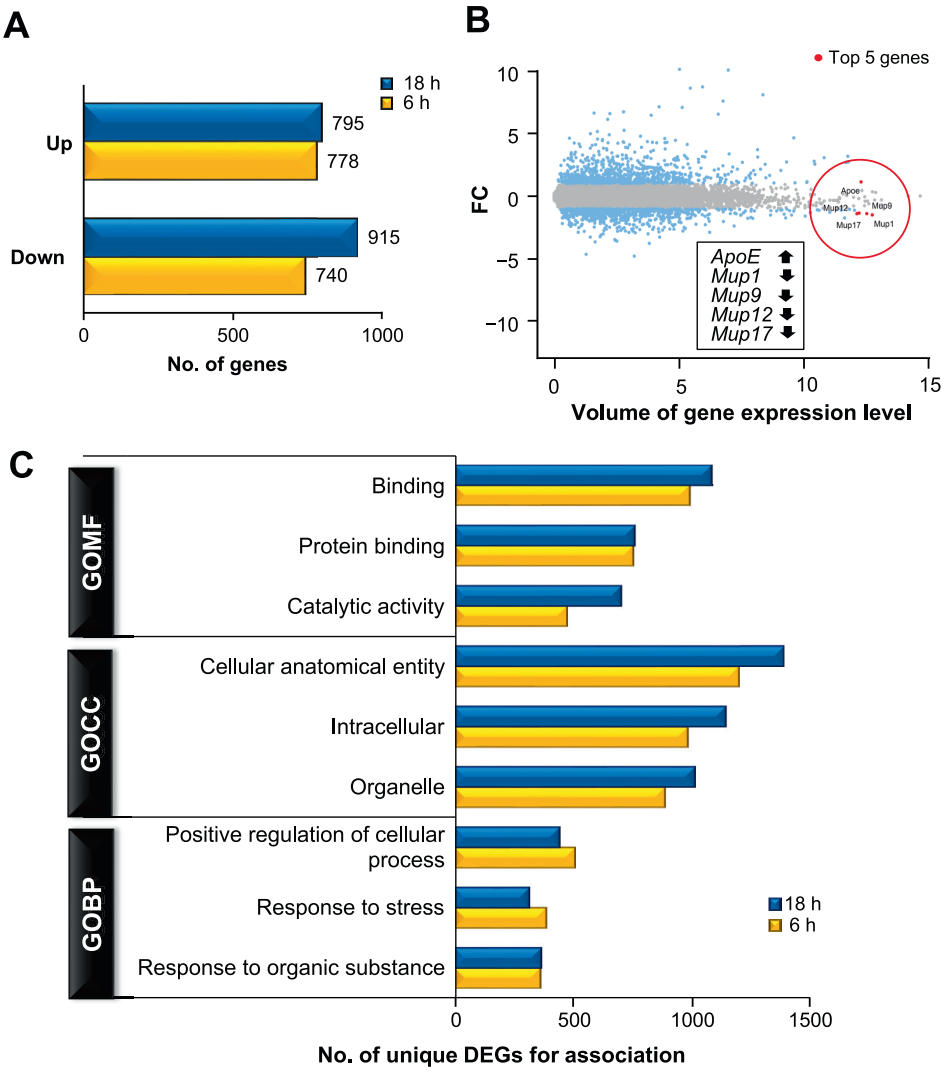

Figure 3 The functional enrichment of transcriptomic profiles in SALD

A. Number of genes with altered expression (FC $\geq$ 2.0 or $\leq$ 0.5) in the 6-h and 18-h CLP groups compared to the 0-h control group. **B.** The top 5 genes considering FC and volume in the 6-h CLP group. **C.** Functional GO analysis of transcriptomes according to the *P* value and intersection size of DEGs (FC $\geq$ 2.0 or $\leq$ 0.5, $P < 0.05$) in the 6-h CLP group. DEG, differentially expressed gene; GO, Gene Ontology; GOMF, Gene Ontology molecular function; GOCC, Gene Ontology cellular component; GOBP, Gene Ontology biological process.

Proteomic analysis reveals association of high-level serine protease inhibitor A3N with inflammation in SALD

To quantify the change in protein level in the livers after CLP surgery, proteins were extracted from livers at 0 h and 18 h after CLP surgery (n = 3 for each group), and each group was pooled for quantitative homogeneity (**Figure 4**A). The pooled samples were divided into two repeated groups and were then analyzed. Each pooled group underwent tryptic digestion in $H_2^{16}O/H_2^{18}O$ to produce $^{16}O/^{18}O$-labeled tryptic peptides and then mixed with 1:1, and comparative proteomic analysis was performed through nano-liquid chromatography-high-resolution tandem mass spectrometry (nano-LC-HR-MS/MS). The association between the duplicate samples was analyzed and Pearson correlation coefficient showed $r = 0.766$ (Figure S5A). The biological samples were normalized with a standardization of the reporter ion intensity value obtained by the median in the histogram shown in Figure S5B. Overall, 3542 proteins were identified of which 2334 were quantified. Among the quantified proteins, 345 proteins showed up-regulated (FC $\geq$ 1.5; n = 206) or down-regulated (FC $\leq$ 0.666; n = 140) expression in the 18-h CLP group, compared to the 0-h control group (Figure 4B; Table S4A).

The significantly differentially expressed proteins (DEPs; FC $\geq$ 1.5 or $\leq$ 0.666, $P < 0.05$) are presented in a Volcano plot, indicating 22 significantly up-regulated DEPs and 20 significantly down-regulated DEPs (Figure 4C; Table S4B). In the up-regulated DEPs, the serine protease inhibitor A3N (SerpinA3N) is a factor related to the expression of inflammation due to aging and high fat, and its increase in SALD is considered reasonable [28,29]. In contrast, major urinary protein 1 (Mup1) was found in the down-regulated DEPs, which is con-

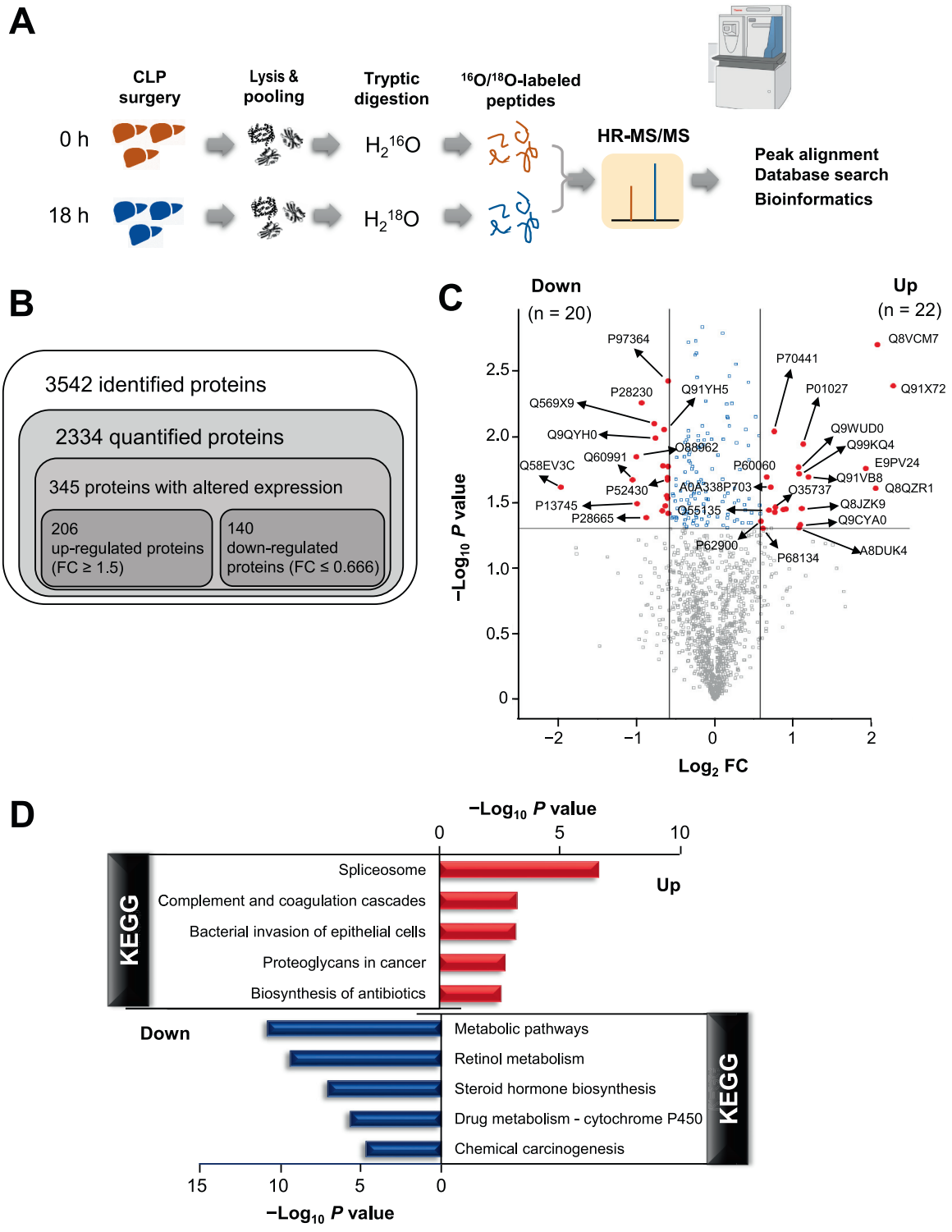

Figure 4 The functional enrichment of proteomic profiles in SALD

A. Experimental scheme for comparative proteomic analysis. **B.** Number of proteins with altered expression (FC ≥1.5 or ≤ 0.666) in the 18-h CLP group compared with the 0-h control group. **C.** Volcano plot showing the significant DEPs (FC ≥ 1.5 or ≤ 0.666, $P < 0.05$) in the 18-h CLP group compared with the 0-h control group. **D.** Enriched KEGG pathways of up-/down-regulated proteins (FC ≥ 1.5 or ≤ 0.666) identified in the 18-h CLP group. Statistical Fisher's exact test values are presented in $\log_{10}$ scale. DEP, differentially expressed protein.

sistent with the decrease of *Mup1* observed in the transcriptome result, thus suggesting that the decreased protein level of Mup1 is due to a reduction in its gene expression level. Because *Mup1* inhibition is linked to increased intestinal epithelial cell permeability, a decrease in the *Mup1* family may influence SALD progression [30].

Both GO and KEGG pathway enrichment analyses were performed using the Database for Annotation, Visualization and Integrated Discovery (DAVID) functional classification tool (Figure 4D, Figure S5C), to understand the functional implication of up-/down-regulated proteins (FC $\geq$ 1.5 or $\leq$ 0.666) in proteomes. For the KEGG pathway enrichment, the up-regulated proteins in the 18-h CLP group were mainly related to spliceosome and complemented and coagulation cascades, and the down-regulated proteins were mainly related to metabolic pathways and retinol metabolism (Figure 4D). In the case of GOMF, RNA binding and aminopeptidase activity were highly enriched for the up-regulated proteins, while heme binding, iron ion binding, and oxidoreductase activity were highly enriched for the down-regulated proteins (Figure S5C). The GOCC annotation was associated with blood microparticles and extracellular exosome for the up-regulated proteins, and with endoplasmic reticulum and intracellular membrane-bounded organelle for the down-regulated proteins (Figure S5C). Furthermore, an association with GOBP was revealed for mRNA processing and splicing in the up-regulated proteins, and for oxidation–reduction process and the epoxygenase P450 pathway in the down-regulated proteins (Figure S5C).

Plasma metabolomic analysis reveals the changes of functional pathways induced in SALD

Plasma metabolomic data were generated by analyzing samples from the 0-h and 18-h CLP groups in biological triplicates (Figure S6). The predicted metabolites with maximum peak area intensity greater than or equal to 1.0×10^6 were included. Consequently, 276 and 116 metabolites were identified from positive and negative modes, respectively (Table S5). Partial least squares discriminant analysis (PLS-DA) validated the classification in the 0-h and 18-h CLP groups (**Figure 5**A). The variables with variable importance plot (VIP) > 1.0 obtained from PLS-DA and/or variables with FC $\geq$ 2.0 or $\leq$ 0.5 and $P < 0.05$ [one-way analysis of variance (ANOVA)] were selected for the verification of the compounds.

Among the 392 metabolites identified in the 18-h CLP group, the contents of 15 metabolites (*e.g.*, leucylproline and glycyl-L-leucine) were up-regulated (FC $\geq$ 2.0, $P < 0.05$), while the contents of 39 metabolites (*e.g.*, nicotinamide and L-tyrosine) were down-regulated (FC $\leq$ 0.5, $P < 0.05$) (Figure 5B). Among these up-/down-regulated metabolites, 22 were identified as differentially expressed metabolites (DEMs) with VIP > 1.0 and FC $\geq$ 2 or $\leq$ 0.5 with $P < 0.05$, including 10 metabolites in the positive mode and 12 metabolites in the negative mode (Figure S6; Table S6). Moreover, these DEMs were selected for pathway analysis using MetaboAnalyst v5.0, the output KEGG pathways were further examined (Figure 5C; **Table 1**). Among the metabolic pathways, "phenylalanine, tyrosine, and tryptophan biosynthesis" and "pantothenate and coenzyme A biosynthesis" in the plasma of the 18-h CLP group were statistically significant ($P < 0.05$). It is well-known that blood phenylalanine increases with protein degradation in severe infection cases, such as sepsis, and it is used as an essential indicator for infection in clinical practice [31,32].

Integrative multi-omics analysis reveals association of Toll-like receptor 4 pathway with SALD

Here, we mainly focused on applying the time-resolved design on a multi-omics approach to detect a response at the pathway level in pathological sepsis (**Figure 6**A). The response time varied considerably within and among the omics datasets due to the variability with the sepsis progression states. Here, an integrative multi-omics dataset was generated, including the phosphoproteomic data from the 4-h CLP liver, the transcriptomic data from the 6-h CLP liver, the proteomic data from the 18-h CLP liver, and the metabolomic data from the 18-h CLP plasma. The time point used for each omics was set according to the reaction sequence of each molecular indicator [21]. All experiments were generated from two or three replicates of each time-course. We relied on FC of each dataset for statistical integration, and aggregated for time point *vs*. its respective control samples. The quantified phosphoproteomic, transcriptomic, proteomic, and metabolomic datasets consisted of 640, 15,323, 2334, 392 molecules, respectively. More specifically, the up-regulated and down-regulated factors were 79:163 (FC $\geq$ 1.5 or $\leq$ 0.666) in the phosphoproteomic dataset, 778:740 (FC $\geq$ 2.0 or $\leq$ 0.5) in the transcriptomic dataset, 206:140 (FC $\geq$ 1.5 or $\leq$ 0.666) in the proteomic dataset, and 15:7 (VIP > 1.0, FC $\geq$ 2.0 or $\leq$ 0.5, $P < 0.05$) in the metabolomic dataset, respectively.

Six cluster algorithms were detected and visualized in integrative network analysis with the xMWAS program v0.55 [33] (Figure 6B) using these datasets. The correlation threshold was set to 0.4, and the number of molecules of multiple datasets in each cluster is shown in **Table 2**. The Reactome database (https://reactome.org/) was used to reveal the top 10 pathways as significantly associated pathways in each cluster ($P < 0.05$) [34] to further explore their respective pathways (Figure S7). Table S7 shows detailed information regarding each biomolecule. In detail, Cluster 1 was highly associated with the Toll-like receptor 4 (TLR4) pathway; Cluster 2 was related to TLR and interleukin signaling regulation; Cluster 3 was related to p53 and iron transport; Cluster 5 was highly associated with the mRNA splicing major pathway; and Cluster 6 was highly associated with solute carrier (SLC) transport, including Slc39a7, Slc30a10, Slc45a3, and Slc41a1. No association with any pathway was found for Cluster 4 due to the small size of its datasets, containg 142 transcriptomes and 4 metabolomes. The detailed gene profiles associated with the top 10 pathways in each cluster are illustrated in Table S7 including the omics source of each biomolecule.

Finally, we summarized the six clusters for integrative analysis, and the total graphical pathway is presented in Figure 6C. During the early stages of sepsis, extracellular HMGB1 binds to TLR4 to induce cytokine production, whereas the intracellular signal can follow one of the two distinct directions: the TLR4/myeloid differentiation primary response 88 (MyD88)/NF-κB and TLR4/Toll/interleukin-1 receptor-domain-containing adapter-inducing interferon-β (TRIF)/Interferon regulatory factor 3 (IRF3) pathways. All the associated layers and their FCs in regulated signaling of multi-omics are shown Figure 6C, respectively. To validate the multiple results involved in SALD, a comparative gene expression analysis

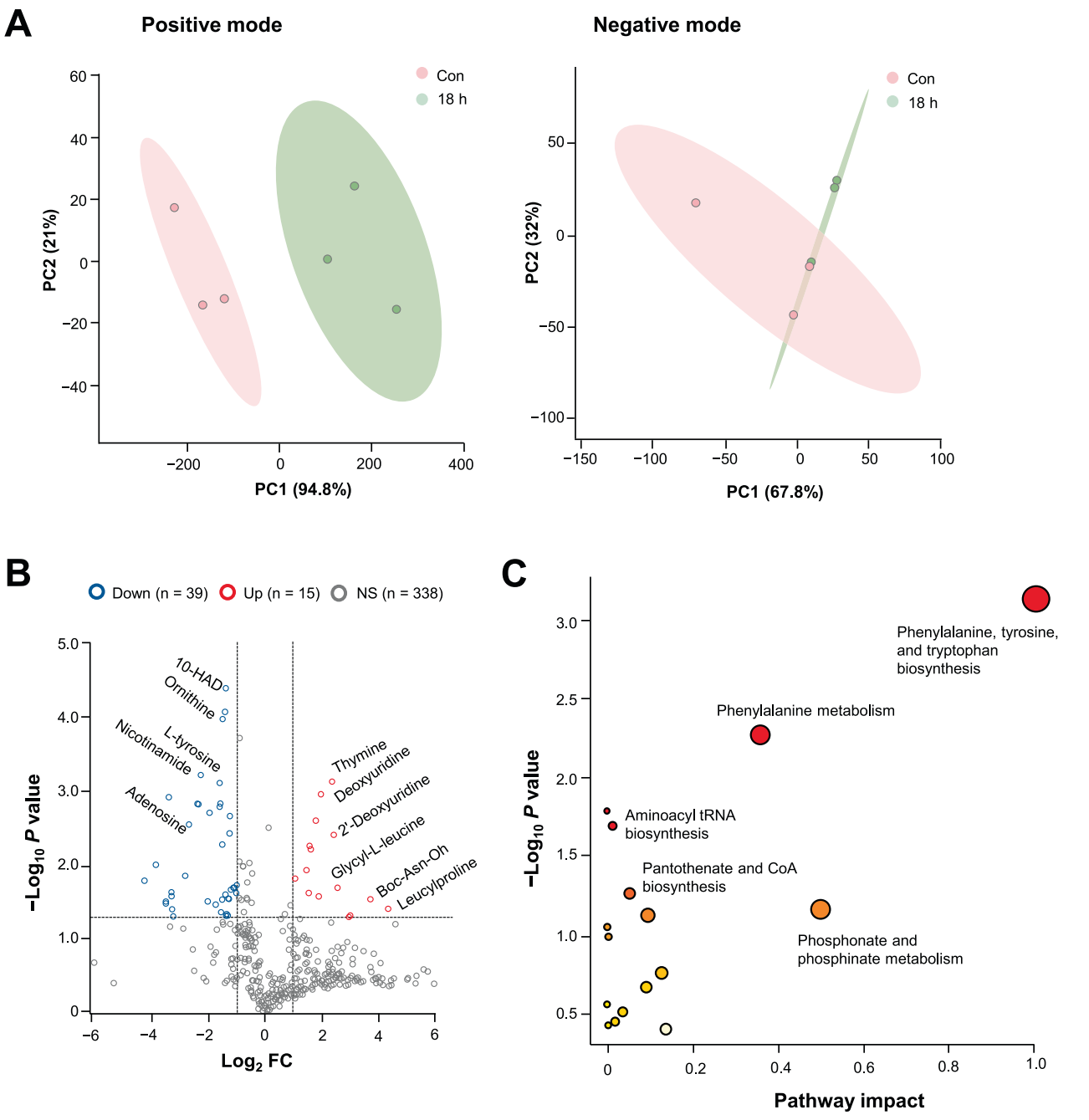

Figure 5 The functional enrichment of metabolomic profiles in SALD

A. PLS-DA of metabolites identified in the positive and negative modes. **B.** Volcano plot showing the distribution of all 392 metabolites identified in the positive and negative modes in the 18-h CLP group. Up means FC $\geq$ 2.0 and $P < 0.05$ (red circles), and down means FC $\leq$ 0.5 and $P < 0.05$ (blue circles). **C.** Enriched KEGG pathways of DEMs (VIP > 1.0 and FC $\geq$ 2 or $\leq$ 0.5 with $P < 0.05$) identified in the 18-h CLP group. Circle color stands for P values ($P < 0.05$, from orange to red), and circle size stands for pathway impacts. PLS-DA, partial least squares discriminant analysis; DEM, differentially expressed metabolite.

Table 1 The information of three KEGG pathways obtained from the plasma metabolomic data at 18 h after CLP

Pathway	Total	Expect	$-\text{Log}_{10}$ P value	Impact
Phenylalanine, tyrosine, and tryptophan biosynthesis	4	0.0465	3.1225	1
Phosphonate and phosphonate metabolism	6	0.0697	1.1688	0.5
Phenylalanine metabolism	10	0.1161	2.2654	0.36

Note: Total means the total number of metabolites or compounds identified from respective pathway. Expect means the expected number of *hits based on the model. *Hit indicates the number of matches in the dataset based on m/z value after mapping to KEGG pathway. KEGG, Kyoto Encyclopedia of Gene and Genomes; CLP, cecum ligation and puncture.

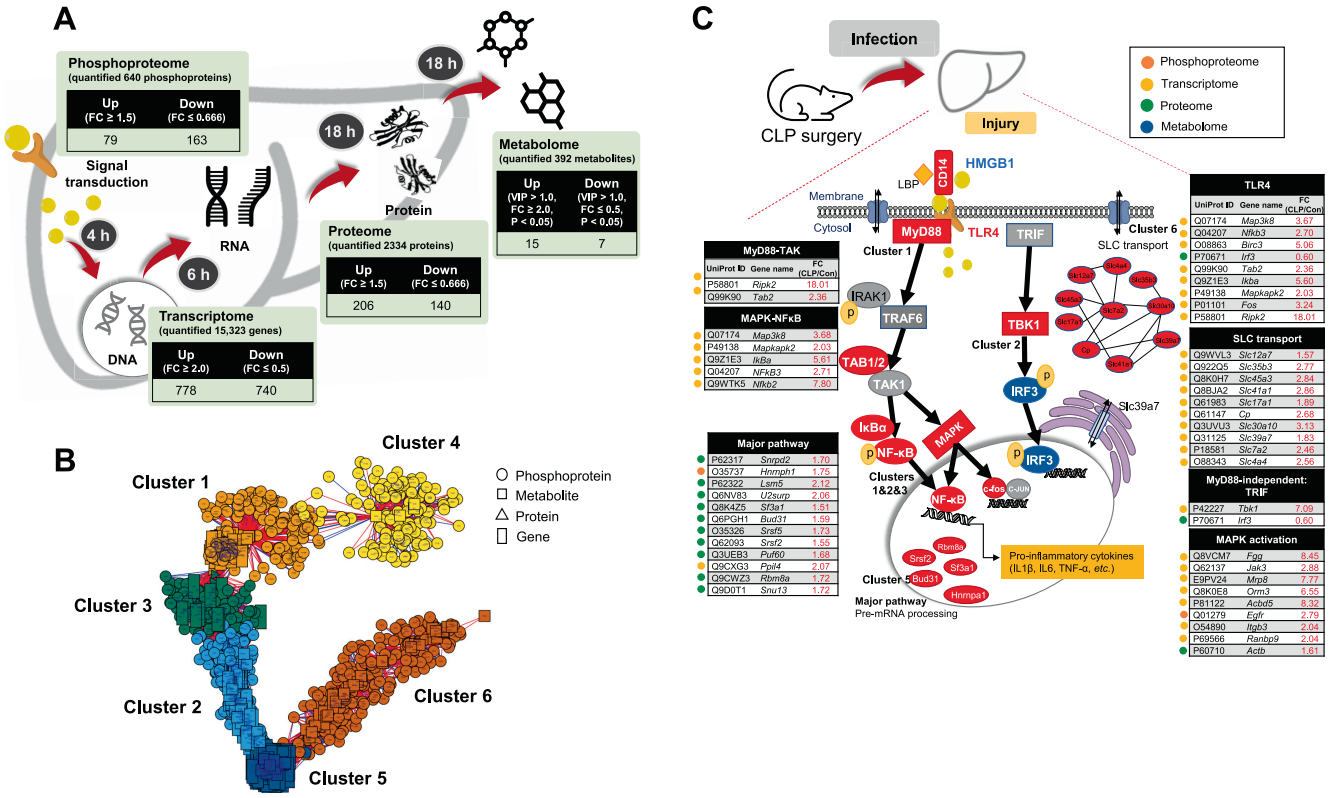

Figure 6 Integrative multi-omics analysis

A. The graphical overview of integrating multi-omics. The number of quantified molecules identified from the phosphoproteomic, transcriptomic, proteomic, and metabolomic data in SALD are also shown. **B.** Integrative network analysis. Using different time-courses of the sepsis model, six community algorithms (Clusters 1–6) were detected by the differently expressed levels of each omics. The xMWAS and network were visualized at a correlation threshold of 0.4. **C.** Graphical pathway from integrative multi-omics communities. The TLR4 pathway is closely related to the MyD88 and TRIF receptor proteins. MyD88 activates TRAF6 with IRAK1 and TAB1/2, and TAK1 facilitated MAPK and IκBα and NF-κB signaling. TLR4, Toll-like receptor 4; MyD88, myeloid differentiation primary response 88; TRIF, TIR-domain-containing adapter-inducing interferon-β; TIR, Toll/interleukin-1 receptor; TRAF6, TNF receptor associated factor 6; IRAK1, IL-1 receptor-associated kinase 1; TAB1/2, TAK1 binding protein 1/2; TAK1, transforming growth factor-β-activated kinase 1; MAPK, mitogen-activated protein kinase; IκBα, nuclear factor of kappa light polypeptide gene enhancer in B-cells inhibitor, alpha; NF-κB, nuclear factor kappa-light-chain-enhancer of activated B cells.

using qRT-PCR was performed to indentify related ten genes in the TLR4 pathway (Figure S8). Ten genes from Clusters 1–3 which were associated with the TLR4 pathway were found to be highly expressed in SALD, which supported the TDMI results. In addition, to characterize the multi-omics changes during TDMI, we also analyzed the distribution of changed genes/proteins among the transcriptomic, phosphoproteomic, and proteomic data via Venn diagram (Figure S9), and the detailed information of these genes/proteins is provided in Table S8. The results showed that eight genes/proteins were shared by these three groups (UniProt ID: Q9ESX5, P70441, Q9R0H0, Q9QYG0, P28230, Q05915, Q99K30, and P58735). Furthermore, 3608, 131, and 200 genes/proteins were transcriptome-, phosphoproteome-, and proteome-specific, respectively. These results suggest that further studies are need to interpret the molecular intricacy and variation at multiple biomolecule levels for these results.

Discussion

In toxicological research, integrative omics analysis has attracted significant attention as a compelling pathway for investigating bodily responses to toxic substance exposure or pathological situations. Recently, technologies for the analysis of each omics, such as genomics, transcriptomics, proteomics, and metabolomics, have rapidly been developed, and it is currently possible to analyze a large number of samples with high sensitivity and high-throughput, thereby producing a considerable amount of results. However, since single-layer omics only provides information on single-type molecules (*e.g.*, gene, RNA, protein, or metabolite), there is a noteworthy limitation while studying toxic molecular mechanisms. Therefore, beyond the study of single-layer omics, studies that integrate and combine information to understand the toxicological mechanisms

Table 2 Number of molecules of multiple datasets in the clusters

Group	No. of molecules					
	Cluster 1	Cluster 2	Cluster 3	Cluster 4	Cluster 5	Cluster 6
Transcriptome	184	187	99	142	77	210
Phosphoproteome	144	34	9	–	72	–
Proteome	27	79	9	–	220	3
Metabolome	4	6	–	4	20	29

across different molecular levels are still in their infancy [21]. Through academic discussions for the application of the "omics" technology to chemical risk assessments, research from biological pathway identification to mode of action and adverse outcome pathway is still ongoing [35].

In our study, several factors related to sepsis could also be identified by a single-omics analysis. Phosphoproteomic data in the 4-h CLP group indicated that the most up-regulated phosphoprotein was pyruvate dehydrogenase E1 alpha subunit (PDHA1a), and the up-regulated phosphoproteins were enriched for the pyruvate metabolism pathway (Figure 2B and C). Pyruvate dehydrogenase plays a vital role in regulating pyruvate oxidation between the glycolysis pathway and trichloroacetic acid (TCA) cycle (citric acid) [25]. The transcriptomic data in the 6-h CLP group revealed *ApoE* as a top up-regulated gene (Figure 3B) that was regulated by an inflammatory factor, which increased during sepsis progression [36]. Proteomic data in the 18-h CLP group revealed 42 significant DEPs (Figure 4C; Table S4B). The highest up-regulated DEP, SerpinA3N, showed an 8.6-fold increase, which has been reported to be involved in multiple vital functions, such as the inflammatory response (TNF-α, IL1-β, and IL-6), and displayed an increased level of SerpinA3N in the sepsis model [37]. Notably, the coding genes of 28 DEPs were also identified to be up- or down-regulated in the transcriptomic data of the 18-h CLP group. In detail, 23 DEPs had the same up-/down-regulated pattern with their gene levels, but different up-/down-regulated patterns between the protein and gene levels were identified in 5 DEPs. In the case of metabolomic data in the 18-h CLP group, the construction of three metabolic pathways in the plasma (Figure 5) demonstrated their importance for host responses to sepsis, such as Phe, Trp, and Tyr biosynthesis, and the Phe metabolism. The early signal in sepsis is the increased level of circulating lactate. Recent studies confirmed the association between high levels of lactate and phenylalanine during sepsis [38]. Another study investigating the metabolic changes in the CLP model suggested reducing IL-6/TNF-α to lower Phe in the sepsis model [39]. The results analyzed by each single-layer omics can explain the critical mechanism associated with sepsis at the level of RNA, proteins, or metabolites. However, the understanding of the integration mechanism that is related to the overall SALD process remains limited.

Therefore, the integration of single-omics results was suggested as an alternative to overcome these limitations. A range of statistical tools and frameworks based on integrating multi-omics were available from many recent reviews [5,16,17,33,35,40]. In the era of big data, the primary issues are to specify the study design for the subsequent integration strategies. Typical omics studies rely on many comparisons and focus on a source-matched studies in which different omics data are generated from the same tissues or cells originating at the same time [41]. However, when considering the information transfer from the external stimuli to the gene, from gene expression to the corresponding protein expression, and the metabolite change due to enzyme expression as the central dogma, a set of several omics data at multiple time points are required to understand a complex disease such as sepsis [42]. Herein, we have mainly focused on applying the time-resolved design on a TDMI approach to detect a response at the pathological-pathway level in the liver with early sepsis. The integrative multi-omics dataset was generated by combining the phosphoproteomic data from the 4-h CLP liver, the transcriptomic data from the 6-h CLP liver, the proteomic data from the 18-h CLP liver, and the metabolomic data from the 18-h CLP plasma (Figure 6A). In this experiment, the final pathways were identified through a two-step integration process. First, a cluster was selected based on integrative network analysis using the xMWAS program v0.55, and the top 10 pathways within the cluster was selected based on the Reactome database. Finally, we successfully deduced that the TLR4 pathway is related to SALD — a well-known signal pathway associated with sepsis based on TDMI data (Figure 6C). The identified TLR4 pathway was verified by qRT-PCR (Figure S8), which revealed a relationship between the dominantly altered genes. During the early stages of sepsis, extracellular HMGB1 binds to TLR4 to induce the production of various cytokines and chemokines [43]. An intracellular signaling can follow either the TLR4/MyD88/NF-κB pathway or the TLR4/TRIF/IRF3 pathway [44]. MyD88-dependent and TRIF-dependent pathways are competitive and mutually exclusive [45]. For further downstream signaling, the adaptor protein MyD88 binds to phosphorylated IRAK1 and TRAF6. Then, it allows the activation of TAB1/TAB2 to promote the phosphorylation of the nuclear factor of kappa light polypeptide gene enhancer in B-cells inhibitor (IκB) complex and the release of NF-κB [46,47]. TAK1 activates various mitogen-activated protein kinases (MAPKs), which together with NF-κB induce the production and release of pro-inflammatory cytokines IL-1β, TNF-α, and IL-6 [48]. The TRIF-dependent pathway leads to TBK1 phosphorylation, thus activating IRF3 via Ser phosphorylation [49]. Other pathways, such as the primary pathways in pre-mRNA processing and SLC transports revealed by the integrative multi-omics analysis, have not been reported in relation to sepsis yet. Although we could not identify the main role of each biomolecule in SALD in this study, another study will be performed to study with in-depth data generated from proteomics, transcriptomics, metabolomics, and epigenomics.

In conclusion, although single-omics analysis provided limited information in this study, a clear pathophysiological pathway, the "TLR4 pathway", was revealed through designated

integration of multi-omics specified in SALD. We agree that several integration challenges remain, including a "gold standard" of unified workflow, sample size, and optimal timing for any omics data. Although present study is limited to present the multi-omics changes of liver, but we do agree that further research should be conducted to examine multi-omics changes in other organs as well, such as lung and kidney tissues, which contribute to the multiple organ dysfunction syndrome. However, the TDMI data showed sufficient utility in predicting the pathological mechanism of disease progression. Furthermore, this can be an ideal paradigm for insightful biological interpretation of multi-omics datasets that will reveal novel insights into basic biology, health, and disease, and insights for the identification of promising candidates for therapeutic strategies.

Materials and methods

Animals, experimental procedures, and treatments

Seven-week-old male ICR mice, weighing approximately 30 g and obtained from Orient Bio. (Seongnam, Republic of Korea), were randomly housed (four mice per cage) upon laboratory arrival under controlled temperature (22 °C–24 °C) and humidity (60%–65%), under a 12-h light/dark cycle. The mice were given standard laboratory chow and distilled water. The mice did not fast before the CLP procedure and were euthanized at different time points after their surgery. Six mice were randomly assigned into five CLP groups (0, 4, 6, 15, and 18 h). Sepsis was surgically induced by the CLP procedure, as previously described [50]. Mice were anesthetized with inhalation of 1.5%–3% isoflurane (Catalog No. P0000KJJ, Hana Pharm, Seoul, Republic of Korea) and were supplied with oxygen gas (O_2) during the CLP surgery. A midline abdominal incision was performed after the abdomen was disinfected and the cecum was exposed. Then, the base of the cecum was ligated and punctured at the distal tip using a 22-gauge needle for midgrade sepsis. A small amount of stool content ($\sim$ 1-mm length) was extruded and put back into the abdominal cavity, and then, the abdomen was sealed in all experimental mice. The control mice underwent the same procedure, but their cecum was neither ligated nor punctured.

Pathological and biological analyses

Whole blood and liver samples from the mice were obtained at 6 h and 18 h after the CLP surgery. Then, the liver tissues were treated in 10% formalin for 24 h. The formalin-fixed samples were embedded in paraffin, and 3–4-μm liver sections were cut. The sections were stained with H&E. Liver injury was assessed by quantification of blood biochemical parameters, including serum ALT, AST, ALP, and LDH, in accordance with the manufacturer's protocols. The damage extent was scored based on severity. According to the percentage area of involvement, multiple liver damage signs (*i.e.*, the amount of destructed hepatic lobules, infiltration of inflammatory cells, hemorrhage, and hepatocyte necrosis) were scored from 1 to 4 per HPF (×400).

RNA extraction and cDNA synthesis

Fifty milligram of liver tissues (n = 6) were homogenized and extracted using the TRIzol Reagent (Catalog No. 15596026, Thermo Fisher Scientific, Waltham, MA) and separated with chloroform (chloroform:TRIzol = 1:5). Then, the same amount of isopropanol was added to precipitate total RNA, which was later washed with 75% ethanol. The RNA pellets were resuspended in 0.1% diethylpyrocarbonate (DEPC) water. Then, cDNA synthesis was performed.

Sample preparation for transcriptome

Total RNA concentration (n = 3) was determined for transcriptome and calculated using the Quant-iT RiboGreen RNA Reagent (Catalog No. R11490, Invitrogen, Waltham, MA). For assessing total RNA integrity, a TapeStation RNA ScreenTape (Catalog No. 5067-5576, Agilent Technologies, Santa Clara, CA) was run, and then high-quality RNA [RNA integrity number (RIN) > 7.0] was used for RNA library construction. One microgram of total RNA was prepared to construct a library using the TruSeq Stranded mRNA Library Prep Kit (Catalog No. RS-122-2101, Illumina, San Diego, CA). The workflow was performed in two steps, including purification of the poly(A) and synthesis of mRNA and cDNA. The cleaved RNA fragments were copied on to the first-strand cDNA and synthesized using the SuperScript II Reverse Transcriptase (Catalog No. 18064014, Invitrogen, Waltham, MA) and random primers. The products were purified and amplified by PCR and quantified using the KAPA Library Quantification Kits (Catalog No. 07960085001, Kapa Biosystems, Waltham, MA) with Illumina sequencing platforms, according to the qPCR Quantification Protocol Guide (Catalog No. KK4854, Kapa Biosystems). The products were validated using the TapeStation D1000 ScreenTape (Catalog No. 5067-5582, Agilent Technologies) to create the final cDNA library. The indexed libraries were submitted to NovaSeq (Catalog No. 2006229, Illumina) and the paired-end (2 × 100 bp) sequencing was performed at Macrogen (Seoul, Republic of Korea).

Sample preparation for global proteome

The extracted protein samples from the liver tissue (n = 3) were reduced with 15 mM dithiothreitol (DTT) in 25 mM ammonium bicarbonate (ABC) at 56 °C for 30 min, and were then immediately alkylated by 60 mM iodoacetamide (IAA) in 25 mM ABC at 25 °C for 30 min. The purified protein precipitation with TCA was quantified with a BCA Kit (Catalog No. A53225, Thermo Fisher Scientific, Waltham, MA). For the enzyme digestion, trypsin (Catalog No. V511A, Promega, Madison, WI) was added with a ratio of 1:50 (w/w, trypsin: protein) and incubated at 37 °C overnight. The CLP group was labeled by oxygen exchange of ^{18}O-enriched water during the trypsin reaction and then mixed with equal amounts of a control group. According to the manufacturer's manual, 100 μg of peptides was fractionated with a different pH elution buffer using a pH reverse-phase column (Catalog No. 84868,

Thermo Fisher Scientific, Waltham, MA). Finally, the eluted peptides were desalted using a C18 ZipTip (Catalog No. 87784, Thermo Fisher Scientific, Waltham, MA) and speed-vacuum dried.

Sample preparation for global phosphoproteome by TiO_2 phosphopeptide enrichment

The peptides (n = 3) purified with Sep-Pak Cartridges (Catalog No. 186000308, Waters, Milford, MA) were prepared, and phosphoproteins were enriched using a High-Select TiO_2 Phosphopeptide Enrichment Kit (Catalog No. A32993, Thermo Fisher Scientific, Waltham, MA). We used TiO_2 spin tips (Catalog No. 87784, Thermo Fisher Scientific, Waltham, MA) with optimized buffer to facilitate preparation in this process, following the manufacturer's instructions. Briefly, 1 mg of peptide samples was put into the TiO_2 spin tips, allowed to bind with the column, and eluted by adding elution buffer after washing. The enriched phosphoproteins were desalted into two types [SDB and GC tips (GL Sciences, Tokyo, Japan)] and speed-vacuum dried. The sample was stored in the −80 °C until further use.

Sample preparation for plasma metabolome

The plasma samples (200 μl, n = 3) were mixed with 1000 μl of methanol and vortexed for 3 min. Then, the sample mixture was centrifuged twice at 13,000 *g* for 10 min at 4 °C. The supernatant was transferred to a new vial and was speed-vacuum dried (Catalog No. 7810010, Labconco Corporation, Kansas City, MO). The dried samples were reconstituted with 150 μl of 20% methanol containing 10 μM fluorenylmethyloxycarbonyl chloride (FMOC)-glycine [internal standard (IS)], and the remaining particles were removed after centrifuging at 13,000 *g* for 5 min at 4 °C. Finally, the supernatant was transferred to LC-MS vials, and 4 μl were injected into the HR-MS.

LC-MS for phosphoproteome and proteome

The labeled and enriched liver samples were individually injected into nano-LC (Catalog No. 320296, Eksigent Technologies, Dublin, CA) connected to an LTQ Orbitrap Velos (Catalog No. 019984, Thermo Fisher Scientific, San Jose, CA) at the Mass Spectrometry Convergence Research Center of the Kyungpook National University. The peptide samples were dissolved in solvent A [0.1% formic acid (FA) in water]. For phosphoproteome, 0% to 90% of solvent B [0.1% FA in 100% acetonitrile (ACN)] was used in gradient elution mode, including 0% to 23% of solvent B for 110 min, 23% to 90% of solvent B for 8 min, and 90% of solvent B for 12 min at flow rate of 300 nl/min. The top 10 data-dependent mode was set to switch automatically between MS and MS/MS acquisition in LTQ Orbitrap Velos. An electrospray voltage of 2 kV was used. A full scan was used for the acquisition of 300–1800 m/z in the Orbitrap with a mass resolution of 60,000. Dynamic exclusion was set to 5 s as repeat duration with a 30-s exclusion duration. For MS/MS, the precursor ions were activated using 27% normalized collision energy at default activation (Q) of 0.25. The desalted peptide mixtures were injected onto the C18 column (4.6 mm × 250 mm, 5 μm; Catalog No. 059149, Thermo Fisher Scientific, Waltham, MA) and fractionated using the HR-MS connected to an UHPLC (Ultimate 3000, Thermo Fisher Scientific, Waltham, MA) in a linear gradient for 0% to 5% of solvent B for 10 min, 5% to 35% of solvent B for 60 min, 80% of solvent B for 12 min, and 5% of solvent B for 25 min. Peptides were loaded onto the trap column and were separated on an analytical column (PepMap RSLC, 3 μm, 100 Å, 75 μm × 50 cm; Catalog No. 164570, Thermo Fisher Scientific, Waltham, MA). The precursor and sequential fragment ions were all measured on a Q-Exactive MS. The MS spectra were ranged from 350 to 1400 m/z and with resolution settings of 70,000 and 17,500 for precursor and sequential fragment ions, respectively, for the data-dependent scan mode.

LC-MS for metabolome

We used HR-MS coupled with an UHPLC (Dionex Ultimate 3000, Dionex Softron GmbH, Germering, Germany) for the metabolomic analysis of plasma samples (n = 3). The LC was composed of an HPG-3200SD (Catalog No. 5040.0021, Thermo Fisher Scientific, Waltham, MA) standard binary pump, a WPS-3000 TRS analytical autosampler (Catalog No. 5826.0020, Thermo Fisher Scientific, Waltham, MA), and a TCC-3000 SD column compartment (Catalog No. 5730.0010, Thermo Fisher Scientific, Waltham, MA) at the Mass Spectrometry Convergence Research Center of the Kyungpook National University. The Q-Exactive Focus Quadrupole-Orbitrap MS (Thermo Fisher Scientific, Bremen, Germany), equipped with a Heated Electrospray Ionization (HESI-II) Probe, was the HR-MS used for identification. Samples were analyzed in both positive and negative modes. As a result, the following optimized positive and negative ion modes were used for the metabolomic analysis of the samples: spray voltage of 3.5 kV for positive ionization mode and 2.5 kV for negative ionization mode, capillary temperature at 320 °C, auxiliary gas at 12 aux units, aux gas heater temperature at 200 °C, sheath gas at 35 aux units, and S-lens radio frequency level of 50 for both ionization modes. The mass resolution was above 70,000 and 17,500 for full MS scan and MS/MS scan, respectively. The data-dependent MS/MS scan procedure was used for the MS/MS scan. The data-dependent MS/MS scan method was optimized with the following parameters: isolation window of 1.4 m/z, collision energy of 30 eV, loop count of 3, and dynamic exclusion of 12 s, and the centroid mode was used to obtain the spectrum data. The elemental composition of all the identified metabolites was determined below 5 ppm as the mass tolerance. A LC column (YMC-Triat C8, 100 mm × 2.1 mm, S-3 μm, 12 nm, column temperature at 40 °C; Catalog No. TO12S03-L5Q1PTH, YMC Korea, Seongnam, Republic of Korea) assisted in separating the endogenous metabolites present in the plasma samples. In addition, all solvents were used and MS grade solvent was mobile phases with a flow rate of 200 μl/min. Solvent A (0.1% FA in water) and solvent B (0.1% FA in 80% ACN) were used in the LC-MS analysis. The gradient elution state for separation was as follows: 2% of solvent B for 5 min, 2% to 50% of solvent B for 8 min, 50% to 95% of solvent B for 4 min, 95% of solvent B for 1.5 min, 95% to 2% of solvent B for 0.5 min, and 2% of solvent B for 2 min.

Database search for transcriptome

All gene expression values were obtained through RNA-seq of *Mus musculus*. The transcript assembly was performed with StringTie v2.1.5 (https://ccb.jhu.edu/software/stringtie/), using the aligned read information. Then, the expression profiles were calculated with the value of FPKM or reads per kilobase of transcript per million mapped reads (RPKM) through the quantified transcripts. For DEGs, functional classification based on GO information was carried out with g:Profiler (https://biit.cs.ut.ee/gprofiler/orth). DEGs were defined as the genes with FC $\geq$ 2.0 or $\leq$ 0.5 and $P < 0.05$.

Database search for phosphoproteome and proteome

We searched all MS/MS spectra against MaxQuant 1.5 with the mice database (released in December 2018). The search parameters were set as follows: tryptic cleavage with two missed cleavage sites, C-termini (+2.0042 Da, +4.0084 Da) for ^{18}O labels, a fixed carbamidomethyl (C) modification and variable modification on acetyl (Protein N-term, +42.0105 Da), oxidation (+15.9949 Da), and phosphorylation (S/T/Y, +79.9663 Da). This software used the calculated $^{18}O/^{16}O$ ratios, allowing accurate quantitative measurement of relative peptide/protein ratios. The search results were filtered with false discovery rate (FDR) < 0.01 and MaxQuant score > 40, thus discarding potential contaminants and results that were only identified by a site modification. Additionally, the cutoff for the probability of the phosphosite localization was set to > 0.75. Following database search, DAVID v6.8 (https://david.ncifcrf.gov/), STRING v11.0 (https://string-db.org/), and Perseus v1.6 were utilized to identify and visualize DEPPs and DEPs. DEPPs and DEPs were defined as the phosphoproteins and proteins with FC $\geq$ 1.5 or $\leq$ 0.666 and $P < 0.05$. The FDR was limited to lower than 0.01. Venny v2.1.0 (https://bioinfogp.cnb.csic.es/tools/venny/) was used to visualize the Venn diagram. The ratio of a protein was defined as the mean of the ratios of all quantified peptides. All experiments were performed as independent biological duplicates. KEGG (https://www.kegg.jp) from DAVID was utilized to predict the related pathways.

Database search for metabolome

All raw data were preprocessed (metabolite identification and peak alignment) using Compound Discoverer 3.1 from Thermo Fisher Scientific (Pittsburgh, PA). Data processing included peak detection and removal of the background matrices. Each peak intensity was normalized using one suitable IS. FMOC-glycine (10 μM) was used as IS for data normalization and quantification of significantly different metabolites among the groups. The data were filtered based on the maximum peak intensity and an m/z cloud match score that was greater than 60 or matched with ChemSpider (https://www.chemspider.com/). The peak shape and MS/MS fragments for each metabolite were also manually confirmed to obtain unbiased results. After searching, a total of 392 metabolites were identified from the positive and negative modes, which were further analyzed by Volcano plot. The metabolites with VIP > 1.0 and FC $\geq$ 2.0 or $\leq$ 0.5 with $P < 0.05$ were defined as DEMs, and utilized for the KEGG pathway analysis with MetaboAnalyst v5.0 (https://www.metaboanalyst.ca/) using the "pathway analysis" option. The output of pathway analysis was examined, and the three KEGG pathways with the highest pathway impacts and lower P values [$P < 0.05$, based on one-way analysis of variance (ANOVA)] were obtained.

Database search for integrative multi-omics data

Data integration from multi-omics and xMWAS (v0.55) from the R software (v4.0.4) were used to infer statistical associations and correlations between layers. A tutorial that includes information related to the installation and usage was provided [6]. xMWAS analysis refers to the pairwise association of up to four datasets based on the sparse partial least squares regression, thus making it possible to illustrate the topology of the datasets integrative network via the calculated association score, and integrate the heterogeneous omics data with many variables and a small sample size. The FCs obtained from the comparison of the expression levels with the control group (0 h) were used for the generation of the data matrices (X, transcriptomic data at 6 h; Y, phosphoproteomic data at 4 h; Z, proteomic data at 15 h; W, metabolomic data at 18 h). The pairwise association was analyzed between X and Y, X and Z, Y and Z, and Z and W, which enabled us to identify clusters of highly associated biomolecules using the multilevel community detection algorithm [17]. The highly associated biomolecules can have functional connectivity [35]. After visualizing the functional clusters from a complex molecular interaction, Reactome (https://reactome.org/) was used to identify the characteristics of each community with $P < 0.05$ [34]. The Reactome software that was used for the analysis of the integrative multi-omics data is a novel and statistically powerful tool for multi-omics pathway analysis. The final raw file from Reactome (a CSV file) was downloaded, and the annotations with $P < 0.05$ were considered as significantly SALD-associated pathways, with the top 10 pathways shown in Figure S7 and Table S7.

Western blotting

Liver tissues (20 mg) were homogenized and lysed in the Radio-Immunoprecipitation Assay (RIPA) buffer, including protease and phosphatase inhibitors (Catalog No. 78442, Thermo Fisher Scientific, Waltham, MA). Protein concentration was determined with Bovine Serum Albumin (BSA; 2 mg/ml) as the standard. Then, protein samples (10 μg) were resolved with 10% acrylamide gel by Sodium dodecyl sulfate polyacrylamide gel electrophoresis (SDS-PAGE), and electrotransferred to polyvinylidene difluoride (PVDF) membrane. After transferring, the membranes were incubated for 1 h at 25 °C in a blocking solution (5% BSA), and incubated overnight with primary antibodies in a washing buffer [Tris-buffered saline (TBS) containing 1% Tween] at 4 °C. The antibodies used were HMGB1 (1:1000; Catalog No. 12029, Abcam, Cambridge, UK), pNF-κB p65 (1:1000; Catalog No. 3033, CST, Danvers, MA), NF-κB p65 (1:1000; Catalog No. 4764, CST), IL-6 (1:1000; Catalog No. 12153, CST), and β-actin (1:1000; Catalog No. 4970, CST). The secondary antibodies used were anti-rabbit IgG (1:2000; Catalog No. 7074S,

CST) or anti-mouse IgG (1:2000; Catalog No. 7076S, CST). Detection was performed using an ECL Kit (Catalog No. PRN2105, GE, Chicago, IL), and the blots were developed using iBright (Catalog No. A44116, Invitrogen, Waltham, MA). The band intensity was quantified with the ImageJ program (https://imagej.nih.gov/ij/).

qRT-PCR

Total RNA was isolated from the mice liver (n = 6) using TRIzol (Catalog No. 15596026, Invitrogen, Carlsbad, CA). First-stand cDNA was synthesized using the SuperScript III First-Strand Synthesis System (Catalog No. 18080051, Invitrogen, Carlsbad, CA). Two nanogram of cDNA template was mixed with SYBR green (Catalog No. 04707516001, Roche, Basel, Switzerland) and primers for amplification. The conditions for PCR amplification were 5 min at 95 °C and 45 cycles of 30 s at 95 °C, 30 s at 58 °C, and 30 s at 72 °C, using the LightCycler 96 Real-Time PCR System (Catalog No. 05–815-916–001, Roche, Basel, Switzerland). Three samples were independently used for quantification. Data were calculated by the $2^{-\Delta\Delta Ct}$ method [51].

Statistical analysis

Data are presented as the mean ± standard error. Results were analyzed using the Statistical Package for the Social Sciences Statistics 26. Differences among groups were evaluated using Student's *t*-tests, and the significance among groups was determined using a one-way ANOVA followed by a Bonferroni's post hoc test. The correlation analysis was performed using a two-tailed Pearson correlation coefficient (*r*). The statistical significance was set at $P < 0.05$, and the differences between categorical data were evaluated using Fisher's exact test. Pearson correlation test was used to investigate the association between the biological replicates of a single-omics dataset.

Ethical statement

The animal experimentation was performed according to the National and Institutional Animal Care and Ethical Guidelines, and was approved by the Institutional Review Board of the Kyungpook National University, Republic of Korea (Approval No. 2020–0127-2).

Data availability

The phosphoproteome/proteome MS data have been deposited in the ProteomeXchange Consortium via the Proteomics Identification Database (PRIDE) partner repository (ProteomeXchange: PXD025800), which are publicly accessible at http://proteomecentral.proteomexchange.org.

Competing interests

The authors have declared no competing interests.

CRediT authorship contribution statement

Ann-Yae Na: Formal analysis, Methodology, Visualization, Writing – original draft. **Hyojin Lee:** Formal analysis, Methodology. **Eun Ki Min:** Formal analysis, Methodology. **Sanjita Paudel:** Formal analysis. **So Young Choi:** Formal analysis. **HyunChae Sim:** Formal analysis. **Kwang-Hyeon Liu:** Conceptualization. **Ki-Tae Kim:** Methodology, Conceptualization. **Jong-Sup Bae:** Formal analysis, Resources. **Sangkyu Lee:** Conceptualization, Writing – original draft, Writing – review & editing, Supervision. All authors have read and approved the final manuscript.

Acknowledgments

This study was supported by the National Research Foundation of Korea funded by the Korean government [Ministry of Science and ICT (MSIT)] (Grant Nos. 2021R1A6A3A01086425 and 2022R1A4A1018900).

Supplementary material

Supplementary data to this article can be found online at https://doi.org/10.1016/j.gpb.2023.04.002.

ORCID

ORCID 0000-0003-0089-3817 (Ann-Yae Na)
ORCID 0000-0002-2945-4415 (Hyojin Lee)
ORCID 0000-0002-8413-5783 (Eun Ki Min)
ORCID 0000-0001-5217-6575 (Sanjita Paudel)
ORCID 0000-0003-3722-967X (So Young Choi)
ORCID 0000-0002-3388-9390 (HyunChae Sim)
ORCID 0000-0002-3285-5594 (Kwang-Hyeon Liu)
ORCID 0000-0002-1130-8698 (Ki-Tae Kim)
ORCID 0000-0002-5756-9367 (Jong-Sup Bae)
ORCID 0000-0001-5343-701X (Sangkyu Lee)

References

[1] Bullock B, Benham MD. Bacterial Sepsis. Treasure Island (FL): StatPearls Publishing; 2022.
[2] Skillman JJ, Bushnell LS, Goldman H, Silen W. Respiratory failure, hypotension, sepsis, and jaundice: a clinical syndrome associated with lethal hemorrhage from acute stress ulceration of the stomach. Am J Surg 1969;117:523–30.
[3] Marshall JC. New translational research provides insights into liver dysfunction in sepsis. PLoS Med 2012;9:e1001341.
[4] Dellinger RP, Levy MM, Rhodes A, Annane D, Gerlach H, Opal SM, et al. Surviving sepsis campaign: international guidelines for management of severe sepsis and septic shock, 2012. Crit Care Med 2013;41:580–637.
[5] Blankenburg M, Haberland L, Elvers HD, Tannert C, Jandrig B. High-throughput omics technologies: potential tools for the investigation of influences of EMF on biological systems. Curr Genomics 2009;10:86–92.
[6] Rohart F, Gautier B, Singh A, Lê Cao KA. mixOmics: an R package for 'omics feature selection and multiple data integration. PLoS Comput Biol 2017;13:e1005752.

[7] Kim M, Tagkopoulos I. Data integration and predictive modeling methods for multi-omics datasets. Mol Omics 2018;14:8–25.
[8] Cui H, Zhou W, Deng Y, Zheng B, Zhang Q, Zhang Z, et al. Meta-transcriptomic profiling of functional variation of freshwater microbial communities induced by an antidepressant sertraline hydrochloride. Sci Total Environ 2021;786:147434.
[9] Kratz M, Coats BR, Hisert KB, Hagman D, Mutskov V, Peris E, et al. Metabolic dysfunction drives a mechanistically distinct proinflammatory phenotype in adipose tissue macrophages. Cell Metab 2014;20:614–25.
[10] Wang F, Li Z, Song T, Jia Y, Qi L, Ren L, et al. Proteomics study on the effect of silybin on cardiomyopathy in obese mice. Sci Rep 2021;11:7136.
[11] Guo J, Zhao J, Liu R, Yu J, Zhang M, Wang H, et al. Metabolomics analysis of serum in pediatric nephrotic syndrome based on targeted and non-targeted platforms. Metabolomics 2021;17:38.
[12] Kempthorne CJ, Nielsen AJ, Wilson DC, McNulty J, Cameron RK, Liscombe DK. Metabolite profiling reveals a role for intercellular dihydrocamalexic acid in the response of mature *Arabidopsis thaliana* to *Pseudomonas syringae*. Phytochemistry 2021;187:112747.
[13] Sindelar RD. Genomics, other "omic" technologies, personalized medicine, and additional biotechnology-related techniques. In: Crommelin DJA, Sindelar RD, Meibohm B, editors. Pharmaceutical biotechnology: fundamentals and applications. New York: Springer; 2013, p.179–221.
[14] Akcakanat A, Zheng X, Cruz Pico CX, Kim TB, Chen K, Korkut A, et al. Genomic, transcriptomic and proteomic profiling of metastatic breast cancer. Clin Cancer Res 2021;27:3243–52.
[15] Graw S, Chappell K, Washam CL, Gies A, Bird J, Robeson 2nd MS, et al. Multi-omics data integration considerations and study design for biological systems and disease. Mol Omics 2021;17:170–85.
[16] Subramanian I, Verma S, Kumar S, Jere A, Anamika K. Multi-omics data integration, interpretation, and its application. Bioinform Biol Insights 2020;14:1177932219899051.
[17] Huang S, Chaudhary K, Garmire LX. More is better: recent progress in multi-omics data integration methods. Front Genet 2017;8:84.
[18] Cavill R, Jennen D, Kleinjans J, Briedé JJ. Transcriptomic and metabolomic data integration. Brief Bioinform 2016;17:891–901.
[19] Buescher JM, Driggers EM. Integration of omics: more than the sum of its parts. Cancer Metab 2016;4:4.
[20] Tarazona S, Balzano-Nogueira L, Conesa A. Multi-omics data integration in time series experiments. In: Jaumot J, Bedia C, Tauler R, editors. Comprehensive analytical chemistry. Amsterdam: Elsevier; 2018, p.505–32.
[21] Canzler S, Schor J, Busch W, Schubert K, Rolle-Kampczyk UE, Seitz H, et al. Prospects and challenges of multi-omics data integration in toxicology. Arch Toxicol 2020;94:371–88.
[22] Liu Y, Ding J, Reynolds LM, Lohman K, Register TC, De La Fuente A, et al. Methylomics of gene expression in human monocytes. Hum Mol Genet 2013;22:5065–74.
[23] Petersen AK, Zeilinger S, Kastenmüller G, Römisch-Margl W, Brugger M, Peters A, et al. Epigenetics meets metabolomics: an epigenome-wide association study with blood serum metabolic traits. Hum Mol Genet 2014;23:534–45.
[24] Shah S, Bonder MJ, Marioni RE, Zhu Z, McRae AF, Zhernakova A, et al. Improving phenotypic prediction by combining genetic and epigenetic associations. Am J Hum Genet 2015;97:75–85.
[25] Rardin MJ, Wiley SE, Naviaux RK, Murphy AN, Dixon JE. Monitoring phosphorylation of the pyruvate dehydrogenase complex. Anal Biochem 2009;389:157–64.
[26] Kattan OM, Kasravi FB, Elford EL, Schell MT, Harris HW. Apolipoprotein E-mediated immune regulation in sepsis. J Immunol 2008;181:1399–408.
[27] Chuang K, Elford EL, Tseng J, Leung B, Harris HW. An expanding role for apolipoprotein E in sepsis and inflammation. Am J Surg 2010;200:391–7.
[28] Boehme M, Guenther M, Stahr A, Liebmann M, Jaenisch N, Witte OW, et al. Impact of indomethacin on neuroinflammation and hippocampal neurogenesis in aged mice. Neurosci Lett 2014;572:7–12.
[29] Dalby MJ, Aviello G, Ross AW, Walker AW, Barrett P, Morgan PJ. Diet induced obesity is independent of metabolic endotoxemia and TLR4 signalling, but markedly increases hypothalamic expression of the acute phase protein, SerpinA3N. Sci Rep 2018;8:15648.
[30] Alaish SM, Timmons J, Smith A, Buzza MS, Murphy E, Zhao A, et al. Candidate genes for limiting cholestatic intestinal injury identified by gene expression profiling. Physiol Rep 2013;1:e00073.
[31] Ten Have GAM, Engelen MPKJ, Wolfe RR, Deutz NEP. Phenylalanine isotope pulse method to measure effect of sepsis on protein breakdown and membrane transport in the pig. Am J Physiol Endocrinol Metab 2017;312:E519–29.
[32] Huang SS, Lin JY, Chen WS, Liu MH, Cheng CW, Cheng ML, et al. Phenylalanine- and leucine-defined metabolic types identify high mortality risk in patients with severe infection. Int J Infect Dis 2019;85:143–9.
[33] Uppal K, Ma C, Go YM, Jones DP, Wren J. xMWAS: a data-driven integration and differential network analysis tool. Bioinformatics 2018;34:701–2.
[34] Sidiropoulos K, Viteri G, Sevilla C, Jupe S, Webber M, Orlic-Milacic M, et al. Reactome enhanced pathway visualization. Bioinformatics 2017;33:3461–7.
[35] Buesen R, Chorley BN, da Silva LB, Daston G, Deferme L, Ebbels T, et al. Applying 'omics technologies in chemicals risk assessment: report of an ECETOC workshop. Regul Toxicol Pharmacol 2017;91:S3–13.
[36] Shao Y, Zhao T, Zhang W, He J, Lu F, Cai Y, et al. Presence of the apolipoprotein E-ε4 allele is associated with an increased risk of sepsis progression. Sci Rep 2020;10:15735.
[37] Gueugneau M, d'Hose D, Barbé C, de Barsy M, Lause P, Maiter D, et al. Increased Serpina3n release into circulation during glucocorticoid-mediated muscle atrophy. J Cachexia Sarcopenia Muscle 2018;9:929–46.
[38] Chiarla C, Giovannini I, Miggiano G. Plasma amino acids of the transsulfuration pathway and plasma lactate in septic patients. Clin Ter 2017;168:e72–6.
[39] Cui Y, Liu S, Zhang X, Ding X, Duan X, Zhu Z, et al. Metabolomic analysis of the effects of adipose-derived mesenchymal stem cell treatment on rats with sepsis-induced acute lung injury. Front Pharmacol 2020;11:902.
[40] Min S, Lee B, Yoon S. Deep learning in bioinformatics. Brief Bioinform 2017;18:851–69.
[41] Misra BB, Langefeld C, Olivier M, Cox LA. Integrated omics: tools, advances and future approaches. J Mol Endocrinol 2019;62:R21–45.
[42] Hasin Y, Seldin M, Lusis A. Multi-omics approaches to disease. Genome Biol 2017;18:83.
[43] Stevens NE, Chapman MJ, Fraser CK, Kuchel TR, Hayball JD, Diener KR. Therapeutic targeting of HMGB1 during experimental sepsis modulates the inflammatory cytokine profile to one associated with improved clinical outcomes. Sci Rep 2017;7:5850.
[44] Shim DW, Heo KH, Kim YK, Sim EJ, Kang TB, Choi JW, et al. Anti-inflammatory action of an antimicrobial model peptide that suppresses the TRIF-dependent signaling pathway via inhibition of Toll-like receptor 4 endocytosis in lipopolysaccharide-stimulated macrophages. PLoS One 2015;10:e0126871.

[45] Guven-Maiorov E, Keskin O, Gursoy A, VanWaes C, Chen Z, Tsai CJ, et al. The architecture of the TIR domain signalosome in the Toll-like receptor-4 signaling pathway. Sci Rep 2015;5:13128.
[46] Wang C, Deng L, Hong M, Akkaraju GR, Inoue J, Chen ZJ. TAK1 is a ubiquitin-dependent kinase of MKK and IKK. Nature 2001;412:346–51.
[47] Ferrao R, Zhou H, Shan Y, Liu Q, Li Q, Shaw DE, et al. IRAK4 dimerization and *trans*-autophosphorylation are induced by Myddosome assembly. Mol Cell 2014;55:891–903.
[48] Akira S, Takeda K. Toll-like receptor signalling. Nat Rev Immunol 2004;4:499–511.
[49] Sharma S, tenOever BR, Grandvaux N, Zhou GP, Lin R, Hiscott J. Triggering the interferon antiviral response through an IKK-related pathway. Science 2003;300:1148–51.
[50] Ebong S, Call D, Nemzek J, Bolgos G, Newcomb D, Remick D. Immunopathologic alterations in murine models of sepsis of increasing severity. Infect Immun 1999;67:6603–10.
[51] Livak KJ, Schmittgen TD. Analysis of relative gene expression data using real-time quantitative PCR and the $2^{-\Delta\Delta Ct}$ method. Methods 2001;25:402–8.